SUPPLEMENTAL DATA

Nbs1 is an Extended Flexible Arm

that binds Ctp1 and Mre11-Rad50

to Coordinate dsDNA Break Processing

R. Scott Williams, Gerald E. Dodson, Oliver Limbo, Yoshiki Yamada, Jessica S. Williams, Grant Guenther, Scott Classen, J.N. Mark Glover, Hiroshi Iwasaki, Paul Russell, and John A. Tainer.

SUPPLEMENTAL EXPERIMENTAL PROCEDURES

X-ray Diffraction Data Collection, Phasing and Refinement

Single crystal X-ray data was collected at the Advanced Light Source (Lawrence Berkeley National Laboratory) on SIBYLS beamline 12.3.1. X-ray data reduction and scaling was performed with the HKL2000 suite (Otwinowski and Minor, 1997).

The apo-Nbs1-fc structure was solved with MAD (Multiple-wavelength anomalous dispersion) with a selenomethionine protein derivative. All 8 Nbs1-fc selenium positions in the crystallographic asymmetric unit of the C-centered orthorhombic cell were located and refined with SOLVE and a 2-wavelength Se-Met dataset (Table S2). Crystallographic phases and experimental electron density maps were further improved by density modification in RESOLVE. Manual fitting in O (v10.0) (Jones et al., 1991) produced a model that was refined to 2.8 Å with REFMAC (Murshudov et al., 1997; Winn et al., 2001) and the MAD dataset remote wavelength ($\lambda 1$) which was collected first and suffered the least radiation damage. Late stages of the refinement utilized TLS group anisotropic B-factor refinement. The final model statistics are detailed in Table S2. Residues 156-158 and 275-286 are disordered in the apo-Nbs1 structure.

Phases for the Nbs1-Ctp1 complex were obtained with molecular replacement using models derived from the apo-Nbs1-fc structure. Because the full spNbs1-fc structure could not be successfully employed in molecular replacement searches, the FHA, $BRCT_1$ and $BRCT_2$ domains were split into pairs or individual domains for use in molecular replacement trials. Solutions were obtained with Phaser (A. J. McCoy, 2007) using FHA-$BRCT_1$ (residues 1-212) and $BRCT_2$ (residues 249-320) search models. This approach identified 3 copies of Nbs1-fc in the crystallographic asymmetric unit (ASU). 2Fo-Fc and Fo-Fc difference electron density and positioning of the search models reveal indicated a large conformational change hinges around the $BRCT_1$-$BRCT_2$ interface, and involves the BRCT linker region. Clear electron density for bound Ctp1 peptide was apparent in one of the three copies in the ASU. One of the other two FHA

peptide-binding sites is clearly blocked and incompatible with peptide binding due obstructive crystal contacts (Figure S5B). The third site is accessible, and may either have very low peptide occupancy (Figure S5C). Model building and refinement was conducted as described for apo-Nbs1-fc. The conformation of the peptide binding loops are found in the closed peptide bound conformation for the other two molecules in the asymmetric unit, consistent with this conformation and associated FHA-BRCT subdomain rotations being linked. In two of three of the Nbs1 copies, a solvent thiocyanate ion is bound that may stabilize the rotated, closed Nbs1 conformation.

The positioning of the flexible loop (aa 155-161) and $BRCT_2$ C-terminal helix α10 shows significant conformational variability between chains and the apo structure that appears dependent on crystal lattice contacts. In chain A of the Nbs1-Ctp1 complex, α10 (residues 303-320) is poorly ordered and has been modeled as polyalanine. The loop encompassing residues 275-287 of all chains in the Nbs1-Ctp1 complex is poorly ordered in the crystal structure and has not been modeled (Chain A) or partially modeled with polyalanine (Chains B and C). A third surface accessible loop is ordered in Chain C, but poorly ordered and not modeled in Chain A (resiudes 256-261) and Chain B (residues 256-258).

Peptide Binding Studies

FITC-labeled peptides absorb at 495 nm and binding of FITC-Ctp1 (Ctp1-1: FITC-KKIQELD(pS)T(pT)DEDEI-nh2) or Ctp1-2: FITC-KKDEIPG(pS)D(pT)VDEED-nh2) to Nbs1-fc was monitored by co-elution in gel filtration. 200 mL protein-phosphopeptide binding reactions containing 150 mM Nbs1-fc (wt or mutant variant), 35 mM Ctp1-1 or Ctp1-2 phosphopeptide in binding buffer (40 mM NaCl, 10mM Tris 7.5, 5% glycerol) were loaded onto a Tricorn Superdex200GL (GE Healthcare). Final protein concentration in eluted peaks is ~8 mM. For unphosphorylated controls, Ctp1-1 and Ctp1-2 peptides were dephosphoylated with 1200 Units of lambda phosphatase (lPPase) (NEB) for 1h at 30 °C.

Fluorescence polarization binding measurements with FITC-conjugated peptides were taken on a Fluoromax-3 (Horiba/Yobin-Yvon) with constant wavelength excitation at 490 nm and emission monitored at 520 nM. Titrations used peptide constant concentration (10 nmol) and increasing amounts of spNbs1-fc protein. Peptides used were doubly phosphorylated Ctp1-1 (FITC-KKIQELD(pS)T(pT)DEDEI-nh2) or the singly phosphorylated derivative (FITC-KKIQELDST(pT)DEDEI-nh2). The unphosphorylated peptide was prepared as for the GF studies. 400 μL binding reactions were equilibrated for 10 min at 20˚C in binding buffer (40 mM NaCl, 20 mM Tris-HCl pH 7.5, 5% glycerol, 0.1 mg/mL bovine serum albumin, 0.1% β-mercaptoethanol) prior to FP measurement. Equilibrium binding constants were calculated with KaleidaGraph (v4.03).

SAXS Data Analysis

Radius of gyration (Rg) and pair distance distribution functions P(r) were evaluated using GNOM (Svergun, 1992). Theoretical scattering for crystallographic structures and MODELLER homology models were generated with CRYSOL (Svergun, 1995).

IR Survival Assays

Surivival assays in response to IR were performed as previously described (Limbo et al., 2007)

SUPPLEMENTAL REFERENCES

A. J. McCoy, R. W. G.-K., P. D. Adams, M. D. Winn, L. C. Storoni and R. J. Read (2007). Phaser crystallographic software. J Appl Cryst *40*, 658-674.

Jones, T. A., Zou, J. Y., Cowan, S. W., and Kjeldgaard, M. (1991). Improved methods for building protein models in electron density maps and the location of errors in these models. Acta Crystallogr A *47 (Pt 2)*, 110-119.

Murshudov, G. N., Vagin, A. A., and Dodson, E. J. (1997). Refinement of macromolecular structures by the maximum-likelihood method. Acta Crystallogr D Biol Crystallogr *53*, 240-255.

Otwinowski, Z., and Minor, W. (1997). Processing of X-ray Diffraction Data Collected in Oscillation Mode, In Methods in Enzymology, C. W. Carter, Jr., and R. M. Sweets, eds. (New York: Academic Press), pp. 307-326.

Svergun, D. I. (1992). Determination of the regularization parameter in indirect-transform methods using perceptual criteria. J Appl Crystallogr *25*, 495-503.

Svergun, D. I., Barberato, C., and Koch, M.H.J. (1995). Crysol—a program to evaluate X-ray solution scattering of biological macromolecules from atomic coordinates. . J Appl Crystallogr *28*, 768-773.

Winn, M. D., Isupov, M. N., and Murshudov, G. N. (2001). Use of TLS parameters to model anisotropic displacements in macromolecular refinement. Acta Crystallogr D Biol Crystallogr *57*, 122-133.

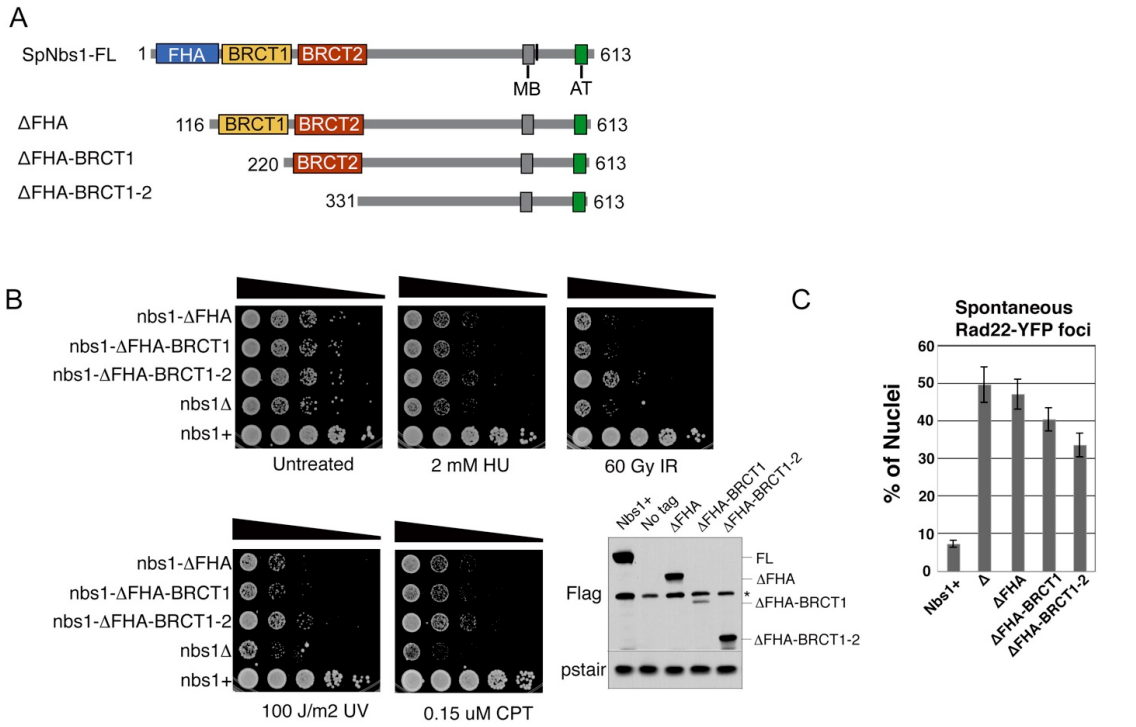

Figure S1. The Structured Nbs1 N-terminal Domain is Required for DSB Repair in *S. pombe.*

A) Nbs1 domain architecture schematic. The Mre11 binding motif is marked with "MB" and the ATM/Tel1 binding motif is marked "AT". (B) HU, IR, UV, and CPT sensitivity assays show that deletion of the spNbs1 FHA domain, FHA-$BRCT_1$ domains, or FHA-$BRCT_1$-$BRCT_2$ domains confers clastogen sensitivity. (C) Nbs1 N-terminal deletions exhibit elevated levels of spontaneous Rad22 foci, indicating increased genomic instability. To assess the importance of Nbs1-fc in DSB repair *in vivo*, we generated spNbs1 N-terminal deletion strains and tested cellular growth efficiency in the presence or absence of genotoxins. The *nbs1-ΔFHA*, *nbs1-Δ(FHA-$BRCT_1$)*, or *nbs1-Δ(FHA-$BRCT_1$-$BRCT_2$)* strains mirror *nbs1Δ* phenotypes. In the absence of genotoxins these phenotypes are characterized by slow growth, elongated cellular morphology and increased $Rad22^{Rad52}$ foci (Figures S2B and S2C). These phenotypes arise from an inability to efficiently repair spontaneous DNA damage, leading to DNA damage checkpoint activation and frequent cell death (You et al., 2005). The Nbs1 N-terminal deletion mutants reduce Nbs1 protein abundance, and display acute sensitivity to the replication inhibitor hydroxyurea (HU), the topoisomerase inhibitor campothecin (CPT), the DNA-crosslinking agent UV, and DSBs induced by ionizing radiation (IR) (Figure S2B).

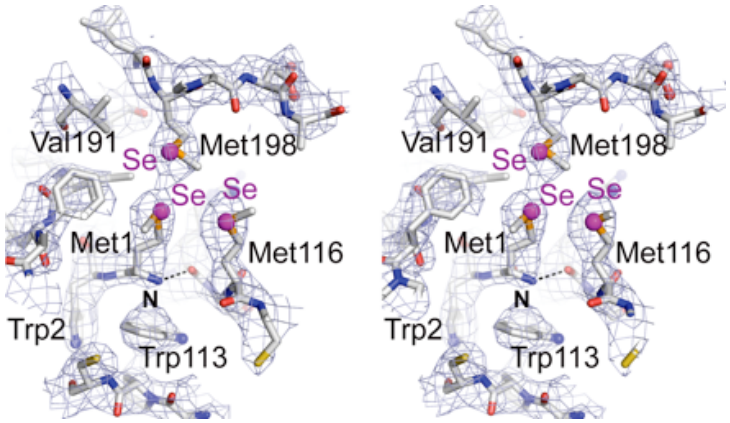

Figure S2. spNbs1-fc Experimental MAD Electron Density Map
MAD-phased and density modified 2.8 Å experimental electron density map is shown contoured at 1.0 σ, overlaid upon a region surrounding the buried Nbs1 N-terminus. A clustering of three closely juxtaposed methionines (Met1, Met116 and Met198) and their Se atom positions (purple spheres) identified with SOLVE are displayed.

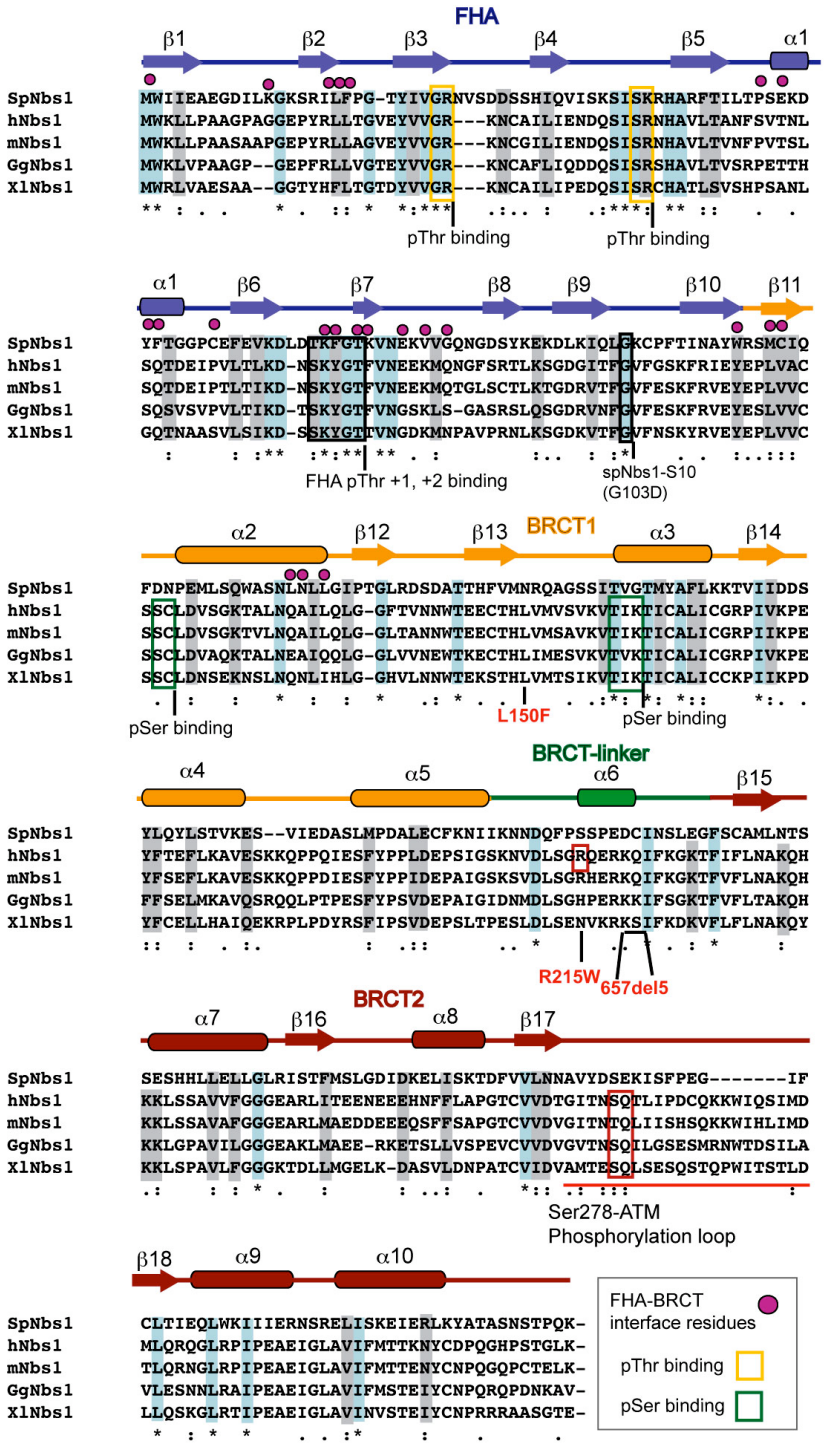

Figure S3. Nbs1-fc structure based sequence alignment
Protein sequences shown are trypsin stable Nbs1-fc fragments from *S. pombe* (SpNbs1, 1-329), human Nbs1 (hNbs1, residues 1-334), and equivalent regions from mouse (mNbs1), *Xenopus laevis* (XlNbs1), amd *Gallus gallus* Nbs1 (GgNbs1). Note: BRCT pSer interaction motifs comprising a conserved S/T at the C-terminus of the first β-sheet in BRCT1 (β11-α2 junction in Nbs1), and a TXK

motif at the N-terminus of the second helix in BRCT1 (α3 in Nbs1) are absent in the *S. pombe* Nbs1 protein, but present in the human, mouse, chicken and Xenopus Nbs1 homologs. The *S. pombe* Nbs1 BRCT domains may therefore participate in phosphorylation-independent protein-protein interactions.

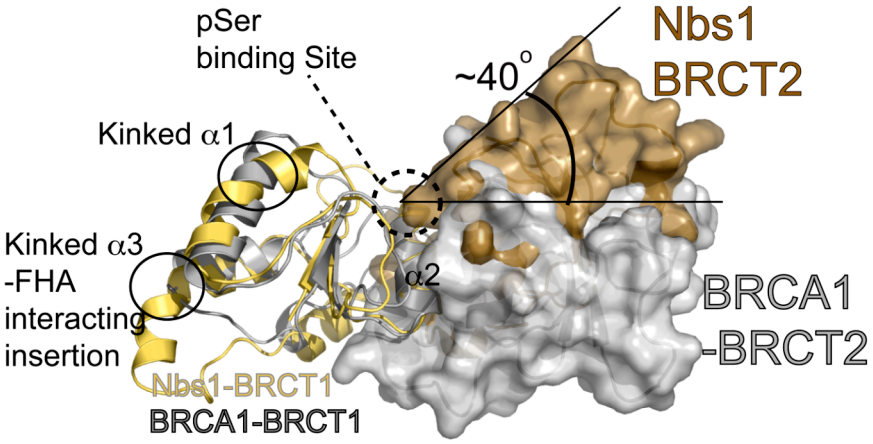

Figure S4. Structural Comparison of spNbs1 and hBRCA1 BRCT repeat structure. The Nbs1 and BRCA1 N-terminal BRCT domains were overlaid using the N-terminal BRCT (BRCT1) of both proteins. Although the inter-BRCT repeat interface is formed via a similar triple helical bundle in both proteins, the inter-BRCT repeat intersection angle is very different between the two proteins. Overall, structural similarities suggest Nbs1 homologs bearing conserved pSer interacting motifs (not *S. pombe)* also bind phosphoproteins via the Nbs1 tandem BRCT domains.

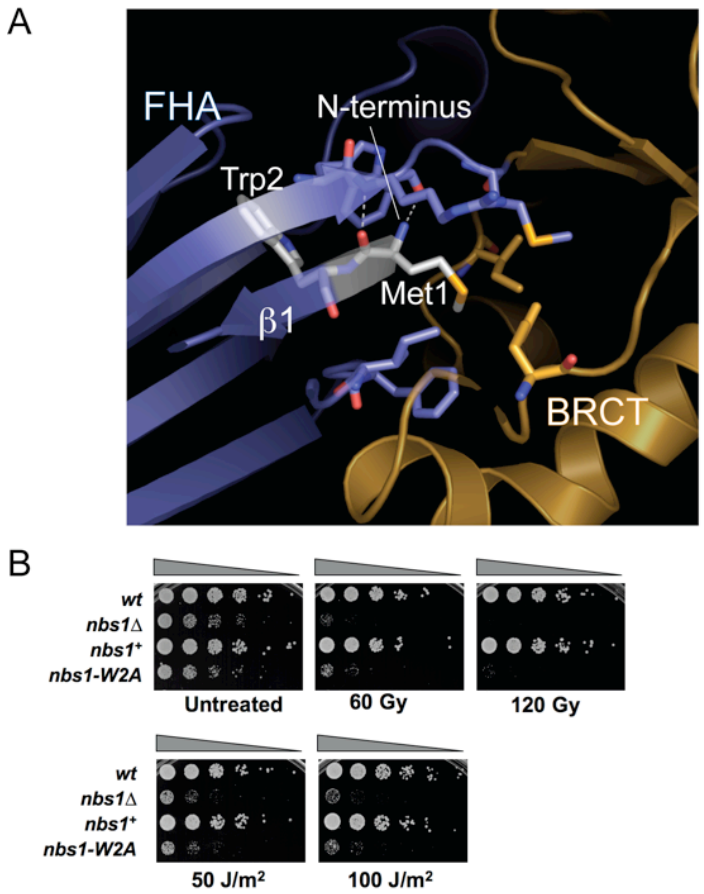

Figure S5. The Nbs1 Buried N-terminus and FHA-BRCT Interface are Critical for *S. pombe* Nbs1 Function

(A) The Nbs1 N-terminal Met is buried in the protein core at the boundary between the FHA domain (blue) and the $BRCT_1$ domain (yellow). Met1 and the invariant Trp2 form the N-terminal end of strand β1.

(B) Mutation of spNbs1 Trp2 confers (*nbs1-W2A*) sensitivity to clastogens, similar to *nbs1Δ* strain.

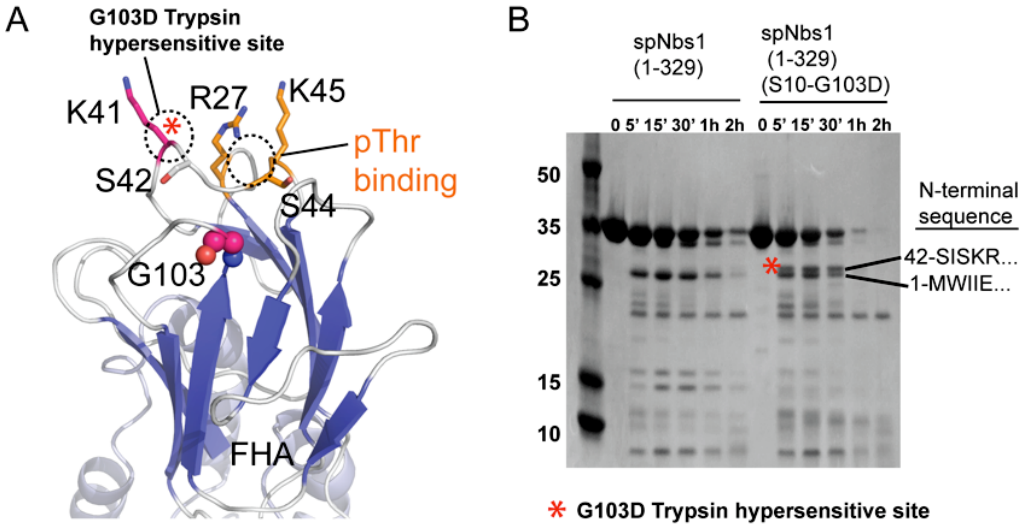

Figure. S6. The Nbs1 S10 Allele (G103D) Destabilizes the Lys45 Peptide-Binding Loop.
(A) Mutation of Gly103 (spheres) to an Asp destabilizes the neighboring peptide binding loop bearing the conserved pThr-contacting residue Lys45. The G103D (S10) substitution introduces a trypsin hypersensitive site at residue Lys41 (red star).
(B) Trypsin degradation of wild-type spNbs1-fc (1-329) and spNbs1-fc-G103D(1-329) shows G103D partially destabilizes Nbs1-fc peptide binding loops, introducing a trypsin hypersensitive site at residue Lys41. Trypsinolysis was conducted at 22 ºC with 50 μg/mL trypsin and 1 mg/mL Nbs1-fc variants and 10 μL aliquots reaction aliquots were taken at the indicated time points and stopped with addition of 1 μL 0.1mg/mL PMSF. The indicated bands were excised and N-terminally sequenced. A red star marks a hypersensitive trypsin cleavage site identified by N-terminal sequencing.

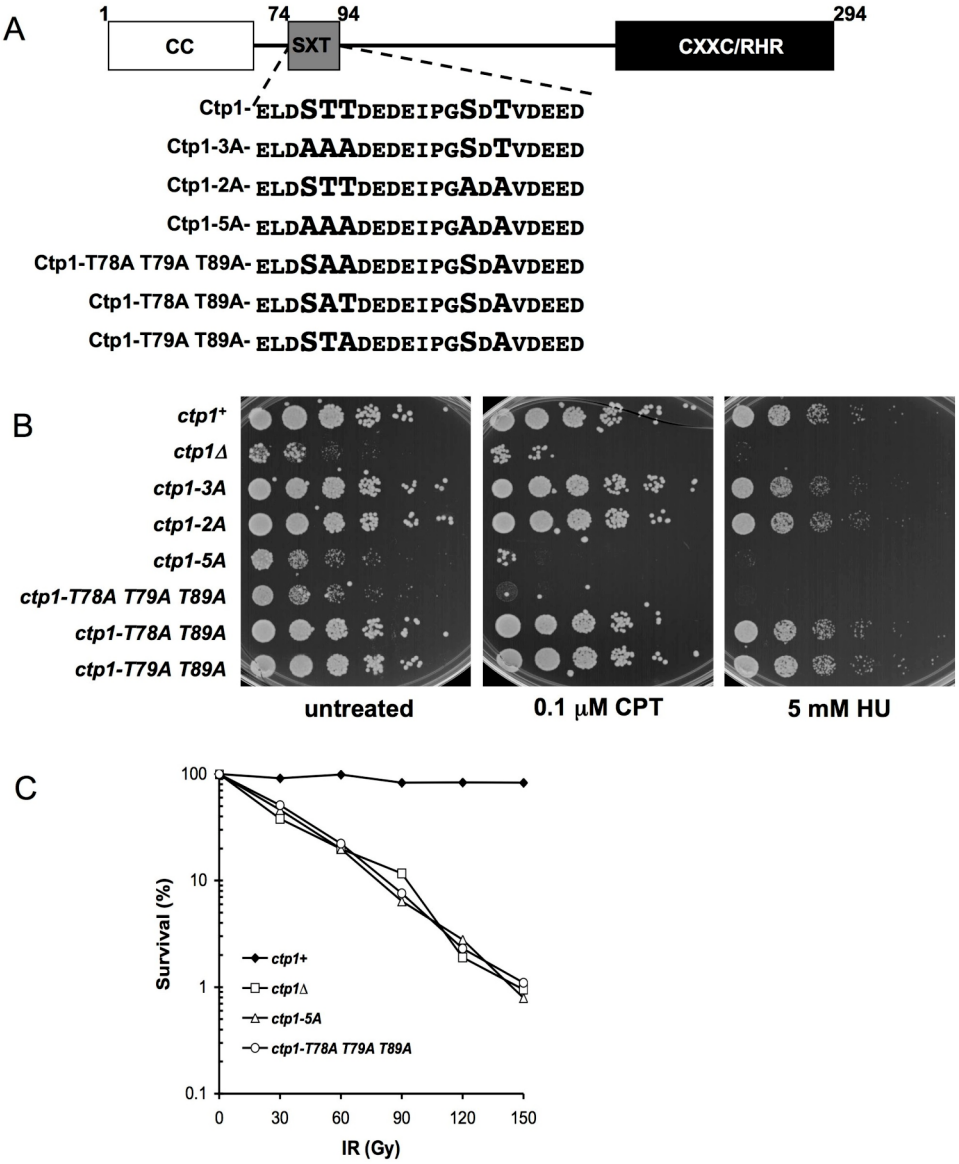

Figure. S7. Mutational dissection of the Ctp1 SXT motifs.
(A) Ctp1 schematic depicting the conserved N-terminal coiled coil domain (CC), C-terminal core homology region (CXXC/RHR), and a putative phosphorylation motif (SXT). An enlargement of this motif shows the amino acid substitutions made in the *ctp1-3A*, *ctp1-2A*, *ctp1-5A*, *ctp1-T78A T79A T89A*, *ctp1-T78A T89A*, and *ctp1-T79A T89A* strains.
(B) *ctp1-T78A T79A T89A* are sensitive to exogenous DNA damaging agents, similar to *ctp1Δ* and *ctp1-5A*.
(C) *ctp1-5A* and *ctp1-T78A T79A T89A* cells are sensitive to IR. Their sensitivity is equivalent to *ctp1Δ*.

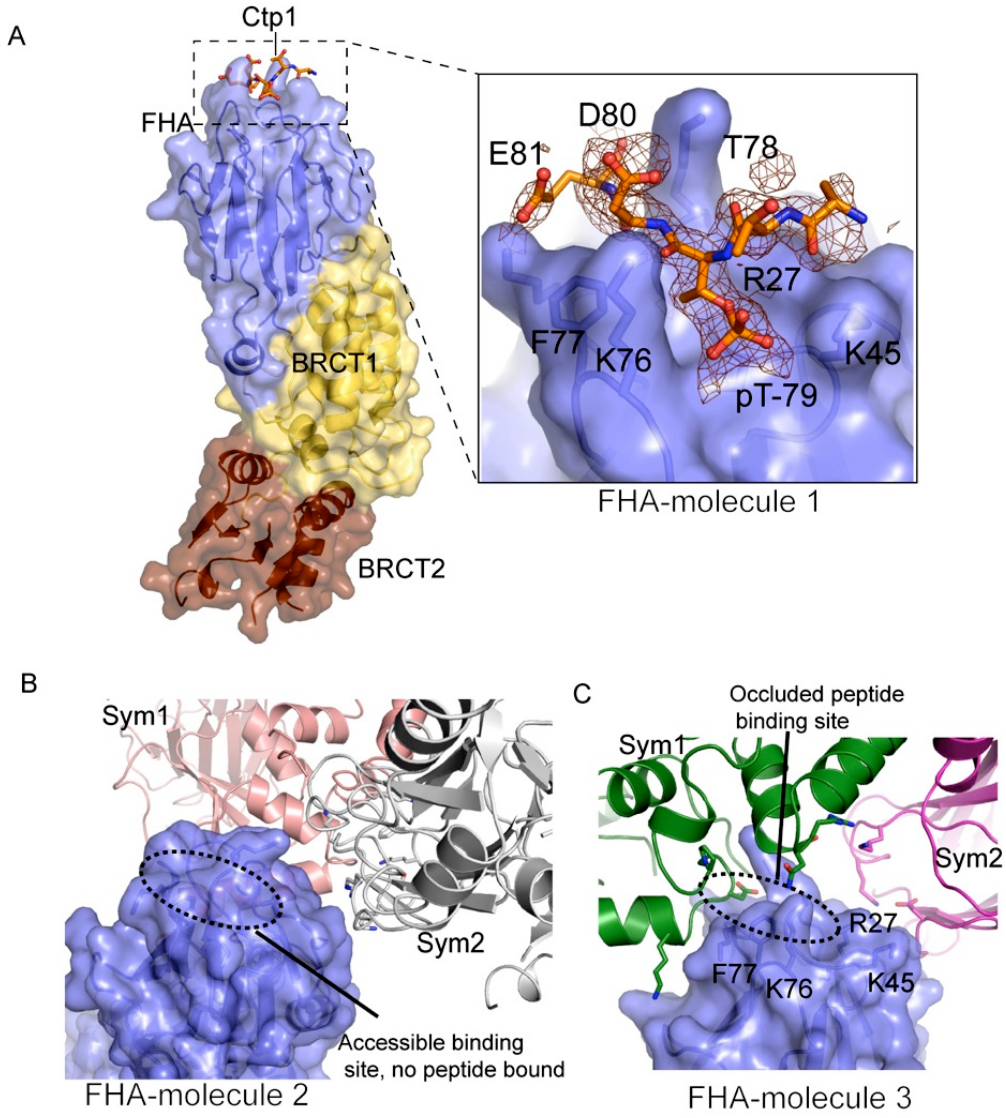

Figure S8. Accessibility of Nbs1 peptide binding sites in the Nbs1-Ctp1 complex crystal form.
(A) Ctp1 binds in the FHA phosphoprotein binding cleft of Molecule 1. Inset: σA-weighted 2Fo-Fc difference density contoured at 0.8 σ (red mesh), and calculated prior to building and refinement of the Ctp1 peptide chain (orange balls and sticks) is displayed overlaid upon the Nbs1 FHA surface (blue).
(B) Molecule 2 contains no bound Ctp1 phophopeptide, but has an apparently accessible FHA peptide-binding site in the crystal. Peptide occupancy may be very low for Molecule 2.
(C) Molecule 3 contains no bound peptide because the FHA peptide-binding pocket is directly occluded by crystallographic symmetry contacts.

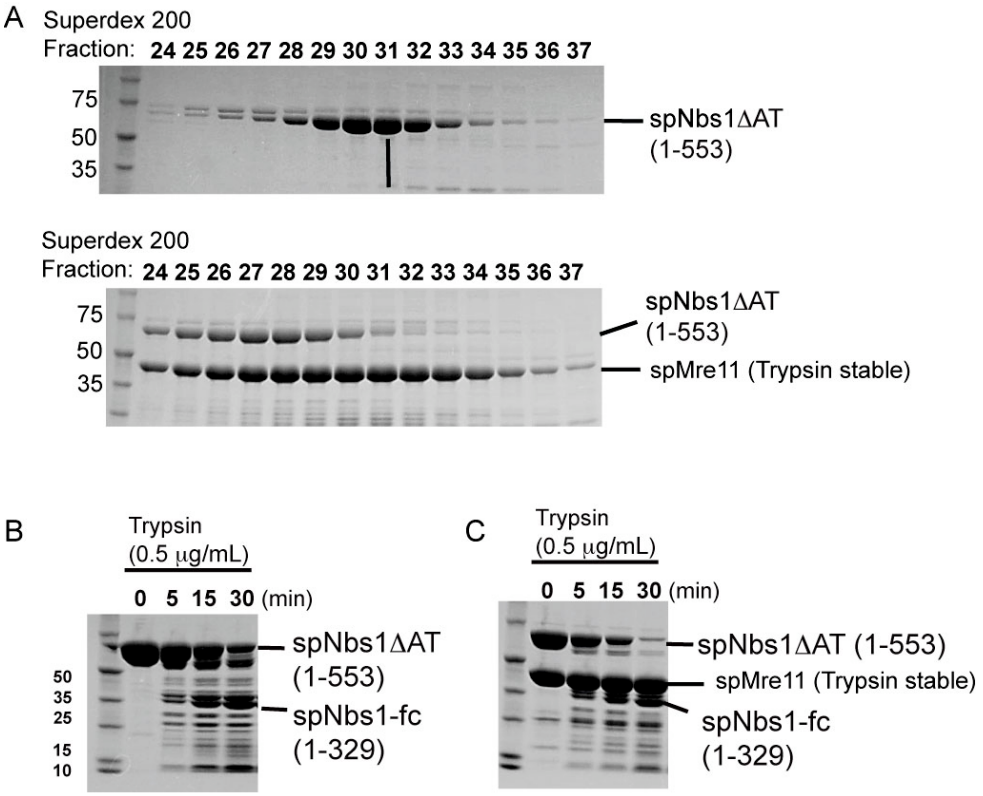

Figure S9 Proteolysis and trypsinolysis of the spMre11/Nbs1 complex.
(A) Superdex200 elution of spNbs1 (1-553). Bottom: Purification of a complex of spNbs1 (1-553) with a trypsin stable spMre11 catalytic domain (B) Trypsinolysis of spNbs1 (1-553) at 4˚C. 0 (C) Trypsinolysis of the Nbs1/Mre11 complex.

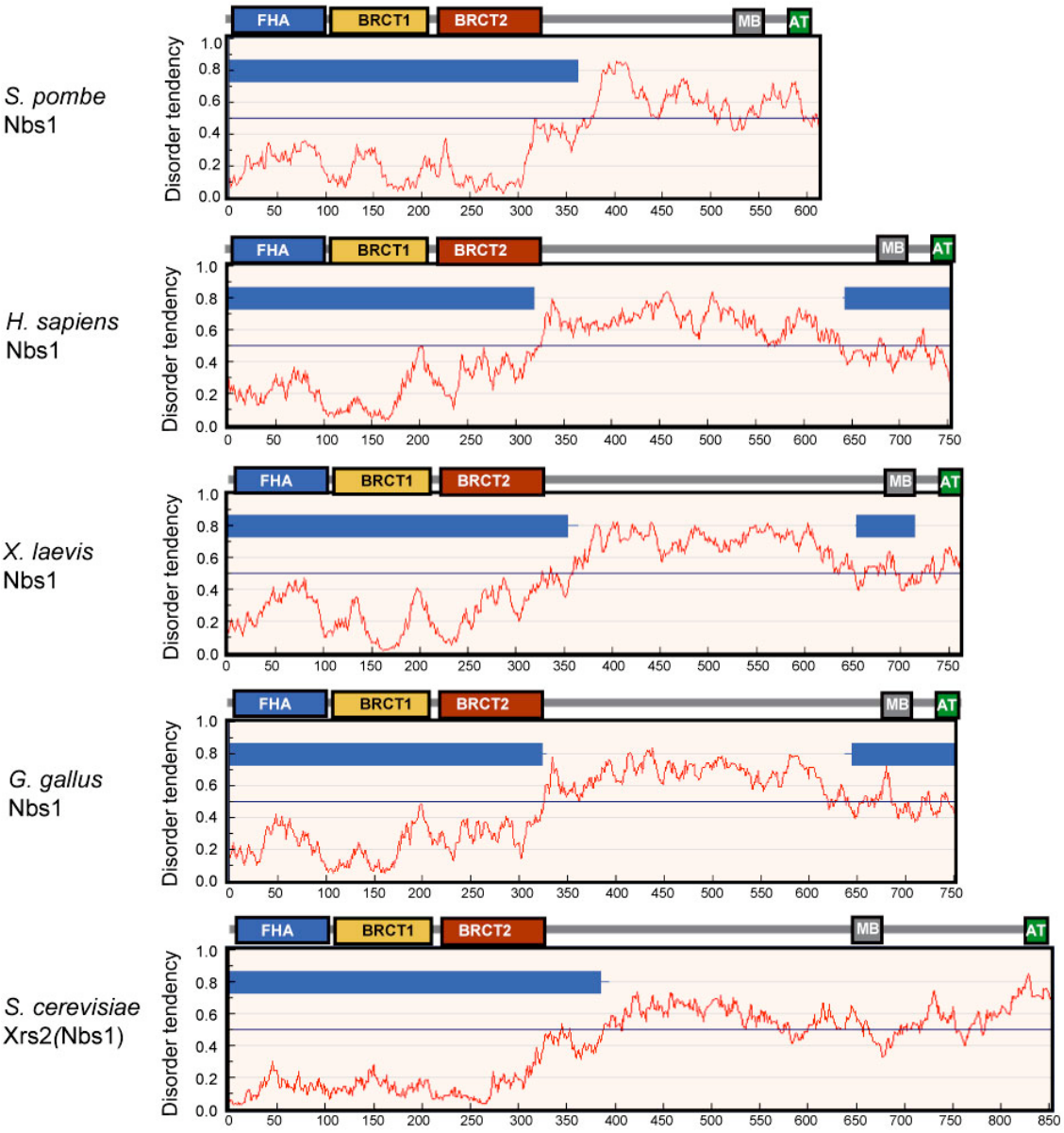

Figure S10. The C-terminal halves of Nbs1 homologs are intrinsically disordered

Predicted ordered domains from IUPRED (http://iupred.enzim.hu/) are shown as blue bars, whereas predicted intrinsically unstructured regions (no blue bars) show stretches of disorder tendency > 0.5. Positions of FHA domain, $BRCT_1$ domain, $BRCT_2$ domain, Mre11 binding motif (MB), and the ATM/Tel1 interacting motif (AT) are marked.

Table S1 *S. pombe* strains used in this study

Strain	Genotype	Source or reference
PR109	*h⁻ leu1-32 ura4-D18*	Lab stock
PR110	*h⁺ leu1-32 ura4-D18*	Lab stock
JW4578	*h? leu1-32 ura4-D18 nbs1::hphMX6 rad22-YFP:kanMX6 his3?*	This study
JW4579	*h? leu1-32 ura4-D18 nbs1-wt-5flag:kanMX6 rad22-YFP:kanMX6 his3?*	This study
JW4580	*h⁻ leu1-32 ura4-D18 nbs1-Δ(FHA-BRCT$_1$)-5flag:kanMX6*	This study
JW4581	*h⁻ leu1-32 ura4-D18 nbs1-Δ(FHA-BRCT$_1$-BRCT$_2$)-5flag:kanMX6*	This study
JW4582	*h⁻ leu1-32 ura4-D18 nbs1-ΔFHA-5flag:kanMX6*	This study
JW4583	*h? leu1-32 ura4-D18 nbs1-ΔFHA-5flag:kanMX6 rad22-YFP:kanMX6 his3?*	This study
JW4584	*h? leu1-32 ura4-D18 nbs1-Δ(FHA-BRCT$_1$)-5flag:kanMX6 rad22-YFP:kanMX6 his3?*	This study
JW4585	*h? leu1-32 ura4-D18 nbs1-Δ(FHA-BRCT$_1$-BRCT$_2$)-5flag:kanMX6 rad22-YFP:kanMX6 his3?*	This study
CC3223	*h⁻ leu1-32 ura4-D18 nbs1::kanMX6*	You et al., 2005
OL4564	*h⁻ leu1-32 ura4-D18 nbs1-5flag:kanMX6*	This study
OL4565	*h⁻ leu1-32 ura4-D18 nbs1-R27A-5flag:kanMX6*	This study
OL4566	*h⁻ leu1-32 ura4-D18 nbs1-K45A-5flag:kanMX6*	This study
OL4567	*h⁻ leu1-32 ura4-D18 nbs1-R27A K45A-5flag:kanMX6*	This study
OL4568*	*h⁻ leu1-32 ura4-D18 nbs1-s10(G103D)-5flag:kanMX6*	This study
OL4569	*h⁺ leu1-32 ura4-D18 rad2::kanMX6*	This study
OL4570	*h⁻ leu1-32 ura4-D18* + pALSK	This study
OL4571	*h⁻ leu1-32 ura4-D18* + pALSK-ctp1	This study
OL4572	*h⁻ leu1-32 ura4-D18 ctp1::hphMX6* + pALSK	This study
OL4573	*h⁻ leu1-32 ura4-D18 ctp1::hphMX6* + pALSK-ctp1	This study
OL4574	*h⁻ leu1-32 ura4-D18 nbs1-R27A K45A-5flag:kanMX6* + pALSK	This study
OL4575	*h⁻ leu1-32 ura4-D18 nbs1-R27A K45A-5flag:kanMX6* + pALSK-ctp1	This study
OL4576	*h⁻ leu1-32 ura4-D18 nbs1-s10(G103D)-5flag:kanMX6* + pALSK	This study
OL4577	*h⁻ leu1-32 ura4-D18 nbs1-s10(G103D)-5flag:kanMX6* + pALSK-ctp1	This study
OL4594	*h⁻ leu1-32 ura4-D18 nbs1-W2A-5flag:kanMX6*	This study
YYY4181	*h? leu1-32 ura4-D18 his3-D1 arg3::HO site(kanMX6) ars1:nmt-(HO endonuclease):ampR:his3⁺:ars1 mre11-H134S-13myc:kanMX6 nbs1-5flag:kanMX6 ctp1-TAP:hphMX6*	Williams et al., 2008
YYY4182	*h? leu1-32 ura4-D18 his3-D1 arg3::HO site(kanMX6) ars1:nmt-(HO endonuclease):ampR:his3⁺:ars1 mre11-H134S-13myc:kanMX6 nbs1-5flag:kanMX6*	Williams et al., 2008
YYY4447	*h? leu1-32 ura4-D18 his3-D1 arg3::HO site(kanMX6) ars1:nmt-(HO endonuclease):ampR:his3⁺:ars1 mre11-H134S-13myc:kanMX6 nbs1-R27A K45A-5flag:kanMX6 ctp1-TAP:hphMX6*	This study
YYY4449	*h? leu1-32 ura4-D18 his3-D1 arg3::HO site(kanMX6) ars1:nmt-(HO endonuclease):ampR:his3⁺:ars1 mre11-H134S-13myc:kanMX6 nbs1-(ΔFHA)-5flag:kanMX6 ctp1-TAP:hphMX6*	This study
YYY4451	*h? leu1-32 ura4-D18 his3-D1 arg3::HO site(kanMX6) ars1:nmt-(HO endonuclease):ampR:his3⁺:ars1 mre11-H134S-13myc:kanMX6 nbs1-s10(G103D)-5flag:kanMX6 ctp1-TAP:hphMX6*	This study
YYY4453	*h? leu1-32 ura4-D18 his3-D1 arg3::HO site(kanMX6) ars1:nmt-(HO endonuclease):ampR:his3⁺:ars1 mre11-H134S-13myc:kanMX6 nbs1::kanMX6 ctp1-TAP:hphMX6*	This study
OL4143	*h⁻ leu1-32 ura4-D18 ctp1-TAP:kanMX6*	Limbo et al., 2007
GD4586	*h? leu1-32 ura4-D18 ctp1-S77A T78A T79A-TAP:kanMX6*	This study
GD4587	*h? leu1-32 ura4-D18 ctp1-S87A T89A-TAP:kanMX6*	This study
GD4588	*h? leu1-32 ura4-D18 ctp1-S77A T78A T79A S87A T89A-TAP:kanMX6*	This study
OL4589	*h⁻ leu1-32::ctp1-3flag:leu+ ura4-D18 ctp1::hphMX6*	This study

OL4590	*h⁻ leu1-32 ura4-D18 ctp1::hphMX6*	This study
GD4591	*h⁻ leu1-32::ctp1-S77A T78A T79A S87A T89A-3flag:leu+ ura4-D18 ctp1::hphMX6*	This study
OL4592	*h⁻ leu1-32 ura4-D18* + pREP41 N-GFP-*ctp1*	This study
GD4593	*h⁻ leu1-32 ura4-D18* +pREP41 N-GFP-*ctp1-S77A T78A T79A S87A T89A*	This study
GD4655	*h⁺ leu1-32 ura4-D18 ctp1-T79A T89A-TAP:kanMX6*	This study
GD4656	*h⁺ leu1-32 ura4-D18 ctp1-T78A T79A T89A-TAP:kanMX6*	This study
GD4657	*h⁺ leu1-32 ura4-D18 ctp1-T78A T89A-TAP:kanMX6*	This study

Table S2. X-ray diffraction data, phasing and refinement statistics

Diffraction data statistics

Data set		**Nbs1 MAD**		**Nbs1/Ctp1 complex**
Synchrotron Beamline		ALS-BL12.3.1		ALS-BL12.3.1
Space group		$C222_1$		$P2_12_12$
Cell dimensions	a (Å)	54.67		97.43
	b (Å)	204.54		244.63
	c (Å)	62.90		52.00
		$\lambda 1$	$\lambda 2$	
Wavelength (Å)		0.9796	0.9797	1.1158
Resolution range (Å)		50-2.80	50-2.80	50-2.15
Observations		71605	70748	227880
Unique reflections		16723	16548	66677
Data coverage total/final shell[1] (%)		99.9/100	99.9/100	97.1/86.6
$\langle I/\sigma I \rangle$ total/final shell		13.9/2.8	13.1/2.5	23.0/2.3
R_{merge} total/final shell (%)[2]		10.0/42.6	10.7/48.1	4.7/43.3

Phasing Statistics
(2wavelength- $\lambda 1$, $\lambda 2$)

Resolution range(Å)	50-2.8
No. of Selenium Sites	8 of 8
Mean FOM - Solve	0.47
Mean FOM - Resolve	0.70

Refinement Statistics		**Nbs1**	**Nbs1/Ctp1 complex**
Resolution range(Å)		50-2.8	50-2.15
R_{work}[3]/R_{free} (%)[4]		23.6/28.5	21.6/26.4
No. of refined atoms	Protein	2429	7249
	Solvent	69	432
Ramachandran (core/allowed/generous)		88.0/10.9/1.1	89.6/9.9/0.5
R.m.s. deviations	Bonds (Å)	0.019	0.012
	Angles (°)	1.758	1.451
Mean B-factors (Å^2)	Protein[5]	33.3	45.6
	Solvent	47.1	47.3
PDB ID		3HUE	3HUF

[1] Final shell: 2.90 – 2.80 Å (Nbs1); 2.23 – 2.15 Å (Nbs1-Ctp1 complex)
[2] $R_{merge}=\Sigma |(I_{hkl}) - \langle I \rangle| / \Sigma(I_{hkl})$ where I_{hkl} is the integrated intensity of a given reflection.
[3] $R_{work} = \Sigma_h|F_o(h) - F_c(h)| / \Sigma_h | F_o(h)|$, where $F_o(h)$ and $F_c(h)$ are observed and calculated structure factors.
[4] R_{free} calculated with 5% of all reflections excluded from refinement stages. No $I/\sigma I$ cutoff was used in the refinement.
[5] B-factors are from individual B-factor refinement following TLS group anisotropic B-factor modeling in REFMAC.